Effect of Processing Conditions on the Structural Gradients Developed in Injection-Molded Poly(aryl ether ketone) (PAEK) Parts. I. Characterization by Microbeam X-ray Diffraction Technique

C. M. HSIUNG and M. CAKMAK*

Institute of Polymer Engineering, College of Polymer Science and Polymer Engineering, University of Akron, Akron, Ohio 44325-0301

SYNOPSIS

Depending on the processing conditions, poly(arylene ether ketone) exhibits unique structural gradients as a result of its thermomechanical history when it is injection-molded. Gapwise structure gradients change from a fully amorphous to multilayer amorphous–semicrystalline–amorphous and, finally, to a uniformly semicrystalline one when mold temperature is increased. When injection speed is decreased, the crystallized layers become thicker, and at very slow injection speeds, the crystalline layers developed near the two surfaces of the parts approach each other at the core. These structure variations were characterized by differential scanning calorimetry, optical microscopy, and a matrixing microbeam X-ray diffraction (MMBX) technique developed in our laboratories. The relationship between the structure gradients developed and the processing variables and the cavity geometry are discussed. © 1993 John Wiley & Sons, Inc.

INTRODUCTION

Injection molding is one of the most commonly used processing operations in the plastics industry. Plastic parts ranging from compact disks to automobile front-end assemblies can be created by this operation. It is one of the most complicated processing operations, which imparts high stresses and rapid cooling to the polymers as they are formed into useful shapes. As a result, the polymeric parts made become highly anisotropic and inhomogeneous in many of their properties. Resin properties, mold geometry, and molding conditions interact to produce a complex thermomechanical history experienced by the resin during the forming operation. As a result, structural features in the injection-molded parts are, hence, complicated and heterogeneous, i.e., they vary with location along the flow direction as well as along the thickness direction. This is especially true for semicrystalline polymers.

There have been many studies concerning the structure development in injection molding of flexible-chain polymers that can crystallize rapidly, like polyethylene (PE),[1-5] polypropylene (PP),[6-9] and polyoxymethylene (POM).[10] But there are a few studies on semicrystalline aromatic polycondensate polymers like poly(*p*-phenylene sulfide) (PPS) or poly(ether ether ketone) (PEEK). These polymers, having a relatively rigid chain backbone, crystallize relatively slowly and the structural features obtained are more sensitive to stress-induced effects. Structure gradients in injection-molded parts of these kind of polymers have been studied by the authors,[11,12] and under certain processing conditions, the amorphous skin–semicrystalline intermediate layer–amorphous core multilayer structures in the thickness direction were found. A computer model that incorporates stress as well as nonisothermal effects on crystallization during and after the flow was developed and successfully applied to prediction

* To whom correspondence should be addressed.

Journal of Applied Polymer Science, Vol. 47, 125–147 (1993)
 CCC 0021-8995/93/010125-23

of crystallinity profiles developed in PPS under a variety of conditions.[13]

Poly(aryl ether ketone)s (PAEKs) are a new kind of aromatic ketone-based high-performance semicrystalline polymers that are heat-stable, chemically resistant, and easily melt-processed. The syntheses of these types of polymers have been reported in the early 1960s[14] and have been followed by many others.[15-23] The chemical composition (ether/ketone ratios) and crystal structure of the PAEK resin used in this study were briefly summarized in our previous paper.[24] These polymers exhibit orthorhombic crystal structure, and when ether and ketone linkages on the polymer backbone are interchanged, the crystal structure is virtually unaffected, as shown by Harris and Robeson.[25]

This paper is part of a series of studies we have been conducting in our laboratories on the processing of semicrystalline high-temperature aromatic polycondensate polymers.[11-13] Structure variations both across and along the flow direction are investigated by optical microscopy. A thorough analysis of crystallinity distribution and crystalline orientation in the thickness direction and at various distances from the gate were studied by DSC and matrixing microbeam wide-angle X-ray diffraction technique (MMBX), which enabled us to map the details of the sharp structural gradients in the parts produced by the injection-molding process. Effects of various processing variables, including mold temperature, injection flow rate, and holding time, are presented.

EXPERIMENTAL

Materials

The polymer used in this study is an extrusion-grade PAEK, KADEL E1000, obtained from Amoco Co. Before injection molding, pellets of as-received unfilled PAEK were dried in a vacuum oven for 12 h at 130°C, then directly used in the injection-molding machine.

Rheological and thermophysical properties of this PAEK material were reported in our previous paper,[24] which included shear viscosity, activation energy of flow, and DSC and TGA data. Flow behavior of PAEK is very similar to PEEK except that the activation energy of the flow of PAEK shows less dependence on shear stress. The glass transition temperature and melting point in a typical DSC trace of rapidly quenched PAEK are 2–3°C higher than those in PEEK. This was used to estimate the ether/ketone ratios in our PAEK polymer[24,25] and our results showed that this PAEK polymer has a mol % ketone linkage of about 38–40%, which is close to the value for poly(ether ether ketone ether ketone) (PEEKEK) reported by Harris et al.[25]

Injection Molding

Tensile bars (Fig. 1) were injection-molded using a Boy (Model 15S) 15 ton reciprocating screw injection molding machine equipped with a standard ASTM test mold and an oil-circulating mold tem-

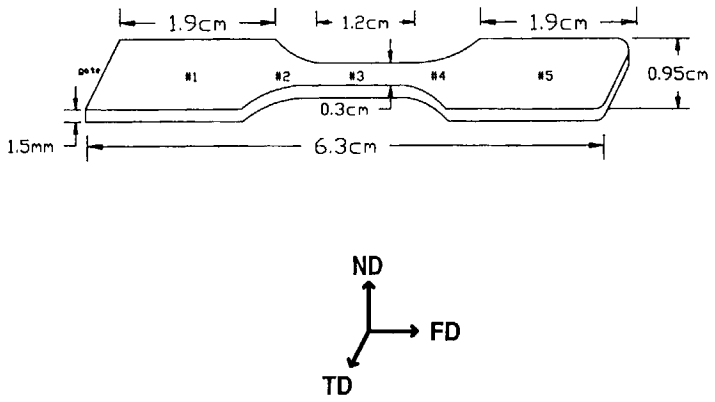

Figure 1 Schematic drawing of the injection-molded specimen showing the locations #1–#5.

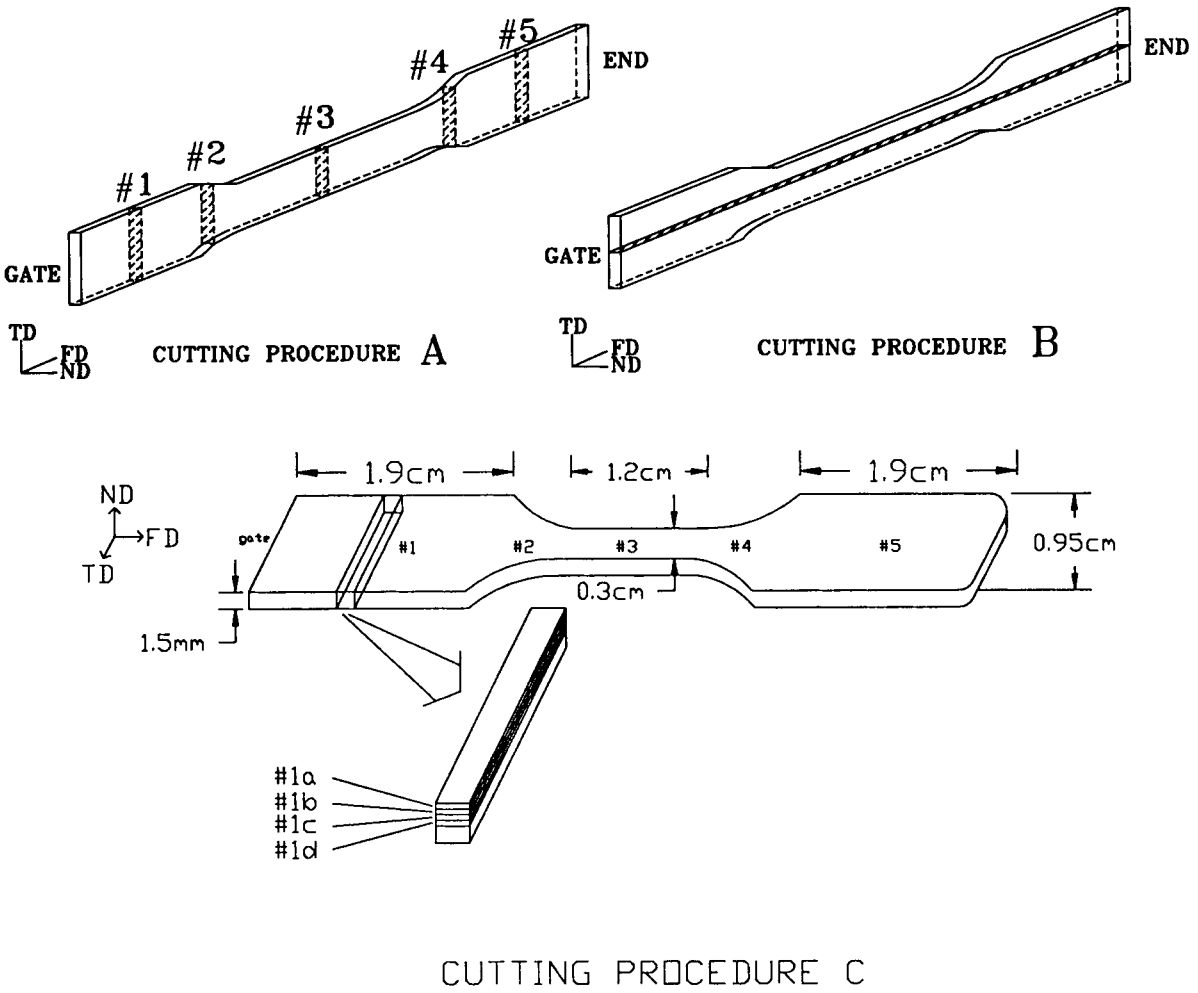

Figure 2 (a) Cutting procedure A; (b) cutting procedure B; (c) cutting procedure for differential scanning calorimetry and X-ray diffraction.

perature controller. The injection speed was monitored by an LVDT (linear variable differential transformer) connected to the screw section on the forward drive.

In this study, the mold temperature as well as the injection speed (injection flow rate) were varied to investigate the effects of processing conditions on the structure variation in the parts. For this purpose, five mold temperatures (20, 70, 115, 150, and 200°C) and two injection speeds (a low speed corresponding to an average flow rate of 5.2 cm^3/s and a high speed of 23.2 cm^3/s) were used. The melt temperature was kept constant at 400°C throughout this study. Both injection pressure and back pressure were kept constant at 13.7 and 1.37 MPa, respectively. In most of our studies, the holding time was kept at 1 min. In a separate study to investigate the effect of holding time, we varied this parameter between 30 s and 10 min at mold temperatures at which thermally activated crystallization becomes significant.

Molded Part Characterization

Sample Sectioning

For direct microscopical observation, samples were cut by a low-speed diamond saw, as shown in Figure 2(a) and (b). Layers of about 0.2 mm in thickness were cut either normal to the flow direction and at different distances from the gate or along the flow direction. These samples are designated as #1–#5 according to their distances from the gate, #1 being the closest and #5 being the farthest from the gate (Fig. 1). In the study of crystallinity distribution

and crystalline orientation in the sample by DSC and wide-angle X-ray diffraction methods, another cutting procedure was used. Here, thin layers of the sample were cut out normal to the thickness direction. This was performed at a minimum of four different levels to obtain detailed variations of crystallinity or crystalline orientation along the normal direction as depicted in Figure 2(c). These layers are named from "a" to "d," with the "a" layer being at the surface and the "d" layer being at the core of the bar.

Optical Microscopy

Because crystalline regions in our injection-molded PAEK samples are opaque while the amorphous regions are transparent, a direct observation of thin slices of the injection-molded PAEK samples under the microscope provides qualitative information on the variation of structure throughout the specimen. For this purpose, a Nikon SMZ-10 microscope was used.

Differential Scanning Calorimetry

Differential scanning calorimetry experiments were performed using a DuPont 9900 DSC with a heating rate of 20°C/min. As mentioned above, samples were cut at different distances from the gate and at different levels from the surface to the core. Then, the crystalline portion of each of these samples was determined from

$$\Delta H_{exp} = \Delta H_{melting} - \Delta H_{cold\ crystallization} \quad (1)$$

Wide-angle X-ray Diffraction (WAXD) Film Patterns

WAXD film patterns on selected samples were obtained by using a Furnas wide-angle and small-angle X-ray camera attached to a GE XRD-6 generator. The generator was operated at 35 kV and 20 mA. X-rays were monochromatized with a nickel foil filter ($\lambda_{CuK\alpha}$ = 1.542 Å). The sample-to-film distance was kept constant at 5.26 cm for all patterns. The exposure time typically was about 6 h. The principal WAXD reflections of PAEK polymer have been found to be the (110) and (200) planes,[24] and by using the flat-film technique and extrapolation method, the unit cell was found to be orthorhombic with a = 7.74 Å, b = 5.96 Å, and c = 10.04 Å,[24] which is consistent with the data reported by Harris and Robeson.[25]

WAXD Film Patterns by Matrixing Microbeam X-ray Camera (MMBX)

A special wide-angle X-ray microcamera with an X–Y sample moving stage was designed and built in our laboratories. The size of the X-ray beam in this camera is about 75 μm, which enabled us to examine the structural gradients through the thickness direction. X-rays are generated by a Rigaku RU-200 12 kW rotating anode generator operated at 40 kV and 150 mA. The beam is monochromatized using a nickel foil filter. The sample is mounted on the X–Y stage and a series of WAXS patterns are taken at desired locations of the sample without dismounting it from the camera; this preserves the spatial registry of each pattern taken with each other. A typical exposure time was about 20 min.

WAXD Pole Figures

To obtain a quantitative orientation distribution in the crystalline regions of molded PAEK, we performed WAXS pole figure analysis. For this purpose, a GE XRD-6 generator equipped with an automated quarter-circle goniometer developed in our laboratories was utilized. Small samples of 0.5 × 0.5 × 0.5 mm^3 in size were cut at various distances from the surface, using a procedure described above, and were mounted on the single-crystal orienter with the spindle axis parallel to the flow direction. The data were acquired with a computer with $\chi = 5°$ intervals and $\phi = 10°$ intervals. Because of the very small size of the samples, counting times as long as 60 s were employed for each interval to improve the signal-to-noise ratio.

In this study, we studied the pole distributions of (110) and (200) crystallographic planes. The normals of (110) and (200) planes are perpendicular to the c-axis (chain axis) and the normal of (200) plane is also along the a-axis.

RESULTS AND DISCUSSION

Effect of Mold Temperature

Here, the effects of mold temperature on the structure variation inside these injection-molded samples are studied by direct observation under a microscope and with DSC methods. Figures 3 and 4 show photomicrographs of dumbbell samples cut normal to the flow direction at location #1. At lower mold temperatures, one can clearly find a three-layer structure made up of a transparent amorphous skin layer, a

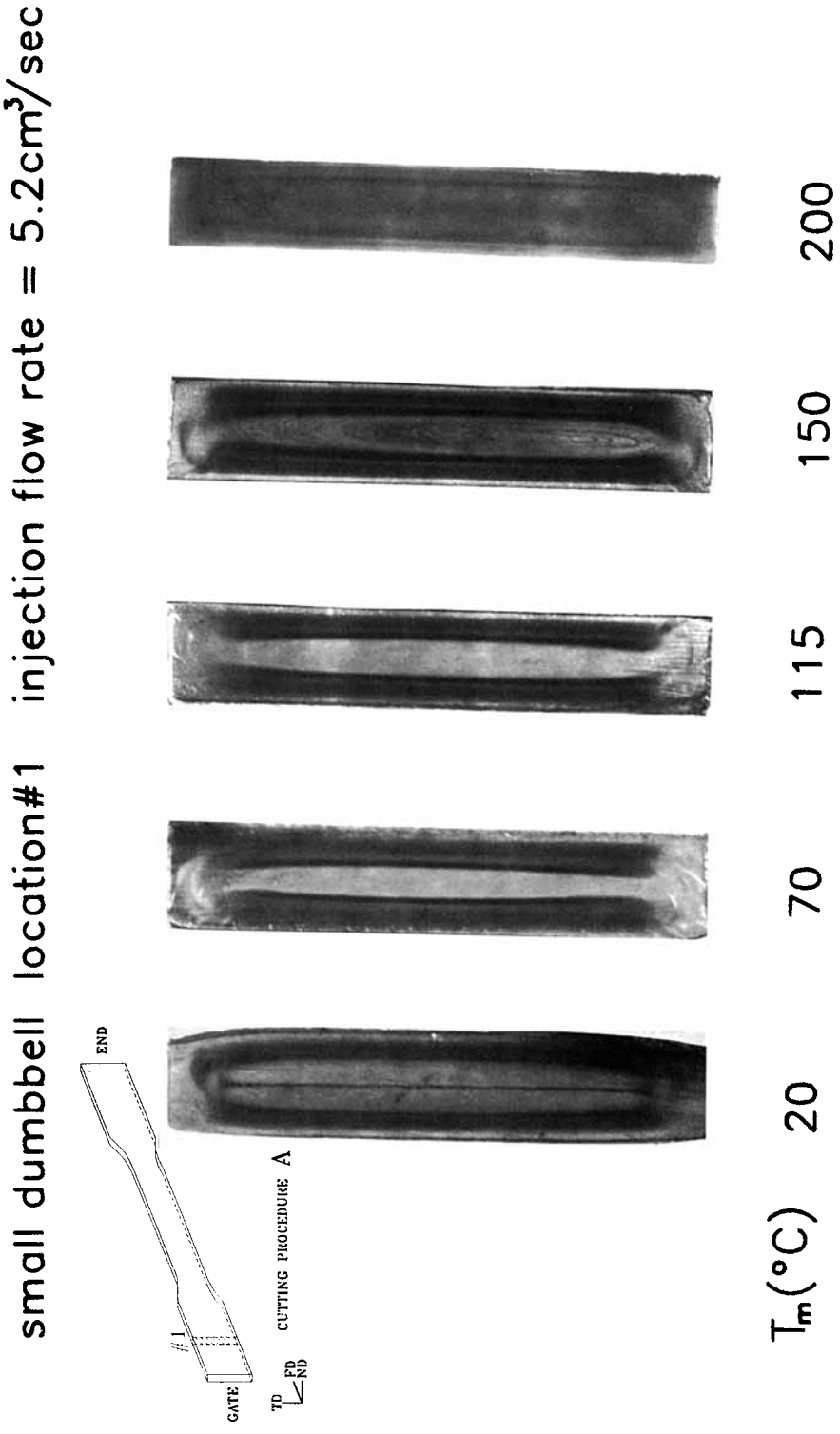

Figure 3 Optical photomicrographs of samples molded at low injection speed and at different mold temperatures and cut at location #1 with cutting procedure A.

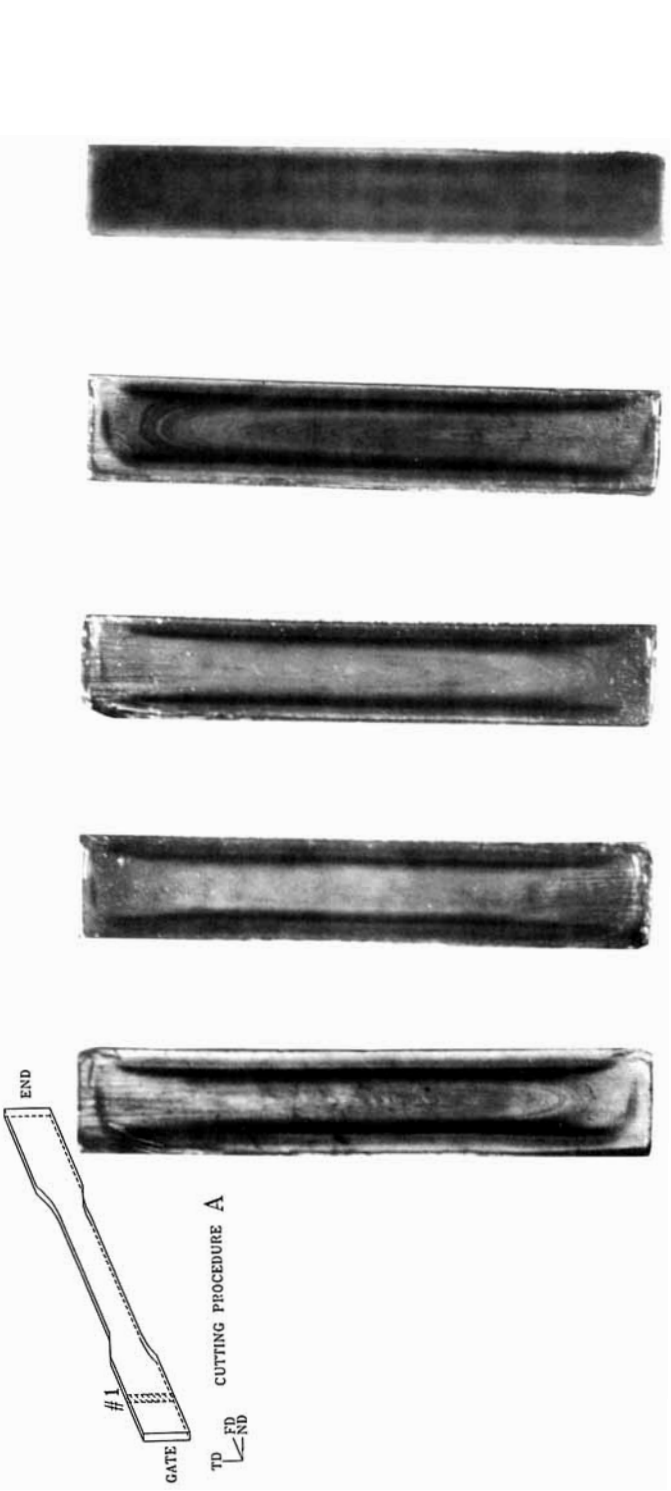

Figure 4 Optical photomicrographs of samples molded at high injection speed and at different mold temperatures and cut at location #1 with cutting procedure A.

darker crystallized zone, and a transparent core. As the mold temperature increases, the thermal crystallization rate increases also, which results in the inner-core regions becoming darker (higher crystallinity), the intermediate crystalline layers becoming thicker, and the transparent amorphous skin layers becoming thinner. At mold temperature of 200°C, sliced samples do not transmit light. The maximum crystallization rate (under isothermal conditions) for this polymer is around 230°C; samples molded at mold temperatures closer to this temperature will have higher thermal crystallization rates throughout most of their thicknesses. In the samples molded at 200°C, we can still distinguish the previously mentioned intermediate crystalline zones by their darker colors. Figure 3 shows photomicrographs for samples molded under low injection speed (average flow rate = 5.2 cm^3/s), whereas Figure 4 shows the high-speed ones (average flow rate = 23.2 cm^3/s). In general, the samples molded at low speeds show thicker intermediate crystalline layers. One interesting point worth noting is the clear dividing line inside the core region of the sample molded at 20°C and under low injection speed. This, as we will show later, is caused by the convergence of two intermediate crystalline layers.

The gapwise crystallinity distributions inside these injection-molded samples was studied by the DSC method (Figs. 5 and 6). For samples molded under 150°C, in general, the crystallinities are low at the skin and core regions and high at the intermediate regions where dark layers were observed in the optical photomicrographs. However, the crystallinity in the sample molded at 20°C with low speed shows a monotonic increase from the skin to

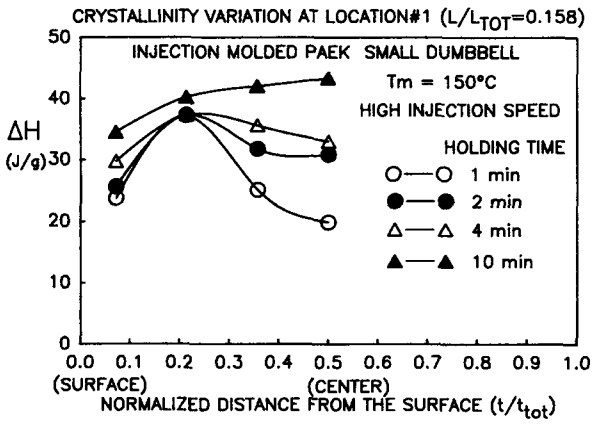

Figure 5 Crystallinity variation from skin to core (center) at location #1 (low injection speed).

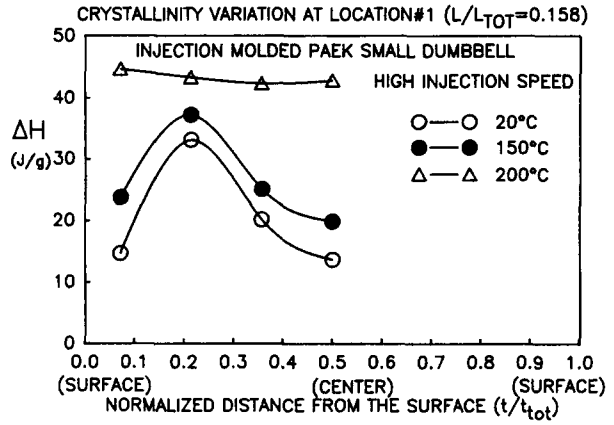

Figure 6 Crystallinity variation from skin to core (center) at location #1 (high injection speed).

the core. This is because the shear stress-induced crystalline layers meet together at this location (Fig. 7). Similar phenomena have been observed in our previous paper about injection molding of PEEK.[12] As the mold temperature is increased, crystallinity also increases as a result of the reduction in cooling rates experienced by the polymer at all distances from the surface. Finally, at 200°C mold temperature, no significant gradient in the crystallinity profile can be observed.

Structure variations along the flow direction in these injection-molded dumbbells are shown in Figures 7 and 8. These samples were cut along the symmetry plane of the sample, as shown schematically on the upper left of this figure. Here, because the samples themselves were used as printing negatives, the original dark regions appear light and transparent lighter regions appear darker. The gate is situated on the left side of the specimens and the vertical direction is the normal direction. In the low-speed case, when the mold temperatures are low (below 150°C), the mold cannot be filled because of premature solidification of the polymer in the mold (short shot) and these samples appear shorter (Fig. 7). At 200°C mold temperature, no short shot behavior was observed. The thickness of the stress-crystallized layers increases downstream and they join together at the midplane in the core. The distance between the gate and the latter merging point increases as the mold temperature is increased. This merging of the crystallized layers in the core is the cause of the premature freezing, which causes the short shot.

At the mold temperature of 200°C, the structure becomes more uniform and only slight structural

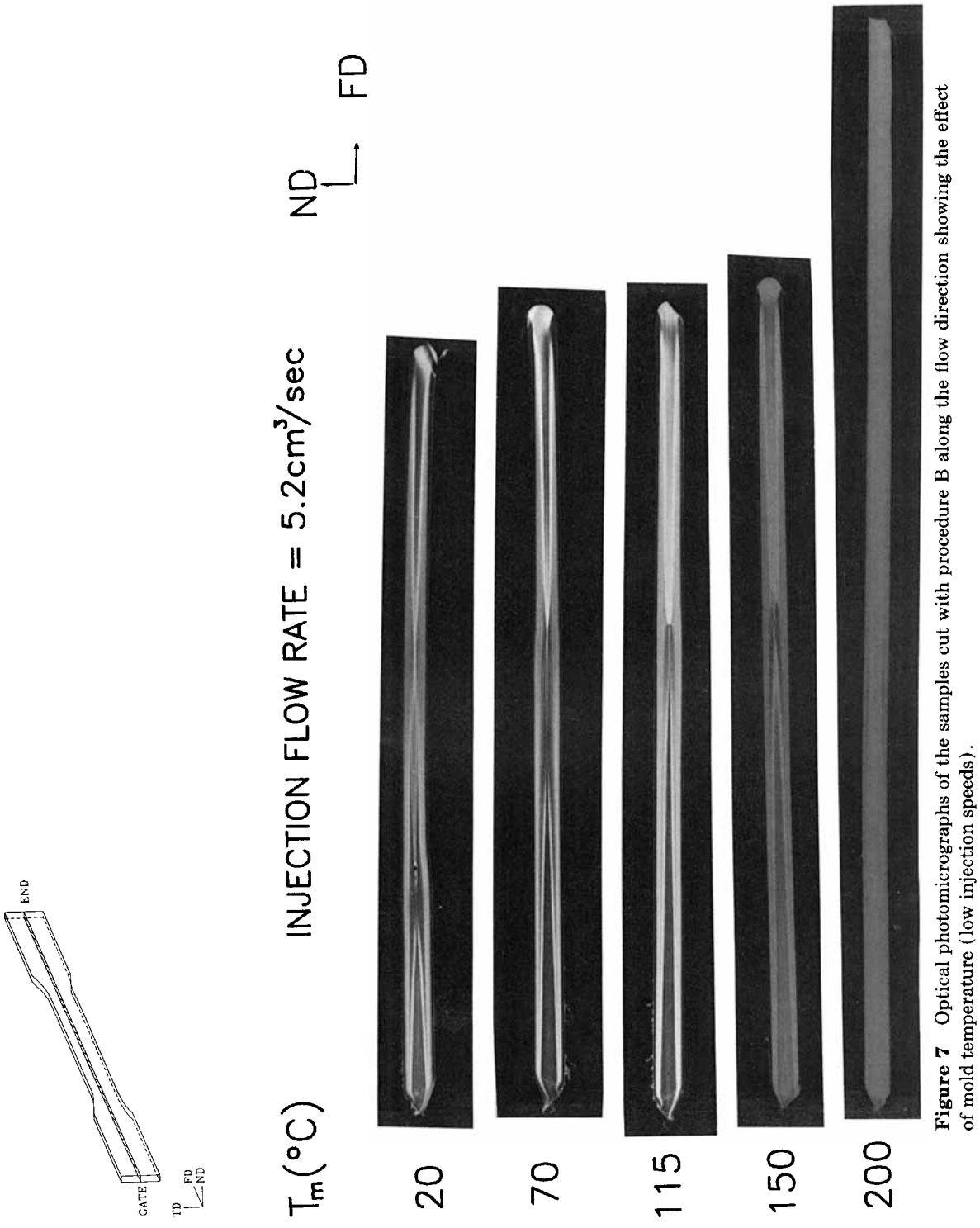

Figure 7 Optical photomicrographs of the samples cut with procedure B along the flow direction showing the effect of mold temperature (low injection speeds).

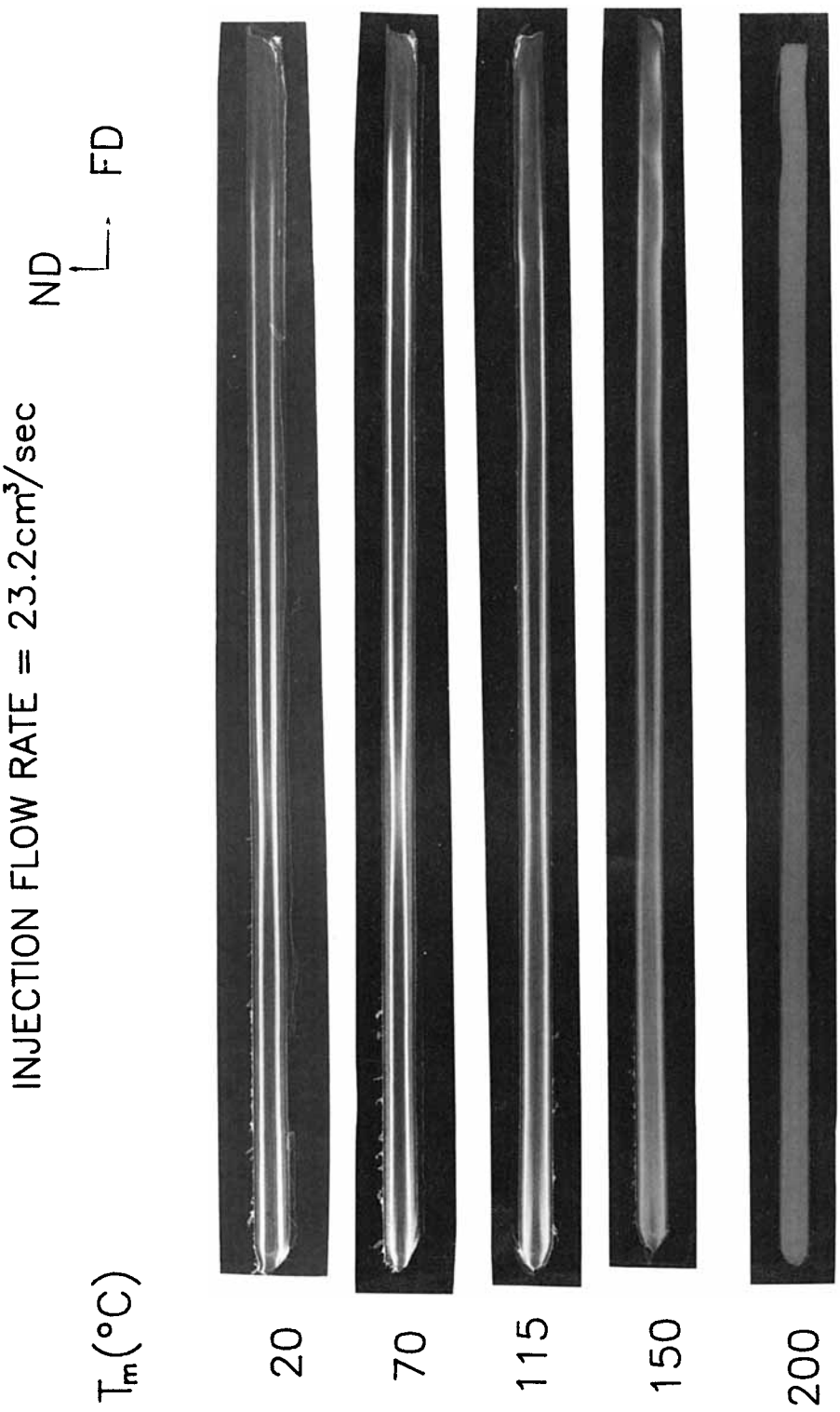

Figure 8 Optical photomicrographs of the samples cut with procedure B along the flow direction showing the effect of mold temperature (high injection speeds).

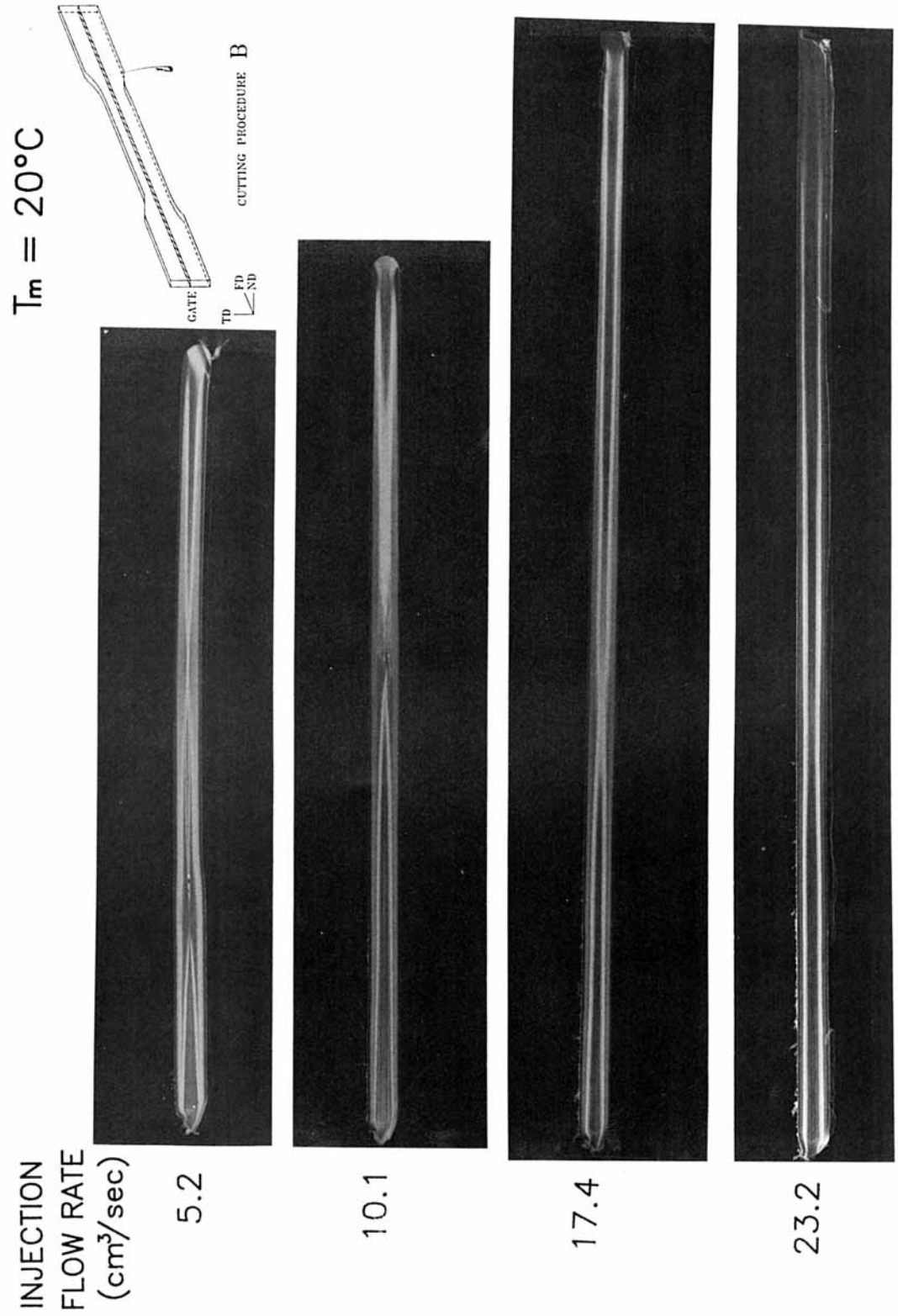

Figure 9 Optical photomicrographs of the samples cut with procedure B along the flow direction showing the effect of injection speed (mold temperature = 20°C).

variations are observed. Samples molded under high speed (Fig. 8) show no short shot. The stress-crystallized layers are smaller in thickness as compared to the samples molded at low injection speed and their thicknesses are more uniform along the flow direction. Although we did not investigate, the mechanical property variation along the flow direction is expected to be more uniform in samples molded with high injection speeds. The two crystallized layers near both surfaces become thicker at about the #2 location where the converging flow takes place. At this region, the extensional component of the flow is maximum due to the accelerative flow (Fig. 1).

Effect of Injection Speed

The operating injection flow rate parameter is important, in that it can be changed rapidly and it can affect the final product properties dramatically. Figure 9 shows the structure variations along flow direction for PAEK material molded at 20°C and under four different injection speeds (samples themselves were used as printing negatives). It is clearly shown that molding at lower injection speeds results in short shot and the interior structure of the resulting parts are much more complicated with multilayer crystalline zones extending to the core regions.

Quantitative DSC results are shown in Figure 10. At 20°C [Fig. 10(a)] mold temperature, the lowering injection speed increases the thickness of crystallized layers. As the mold temperature is increased [Fig. 10(b)], the influence of stress-induced crystallization becomes less and we have the typical three-layer structure with the highest crystallinity observed at the intermediate depths, but samples molded at lower speed still possess a higher and broader crystalline zone and crystallinities in their core regions are higher compared to samples molded at higher injection speed. Finally, at the highest mold temperature of 200°C where thermally activated crystallization is dominant, the effect of injection speed is minimal [Fig. 10(c)].

There are two factors that are responsible for the effects of the injection flow rate. The first one is the formation of frozen layers during the filling stage, which reduce the channel thickness and increase the velocity and shear rate in the near-core region. The second factor is that filling time is increased by reducing the injection flow rate. Because this is also the time that the polymer is under stress, reducing injection flow rate imparts to the polymer melt a longer shearing time while it is cooling. In addition, the stresses are increased with the increase of filling time, because longer filling means longer cooling during flow, and longer cooling in our thin mold geometry can result in a significant decrease in melt temperature and, thus, cause a substantial increase in viscosity. The crystallized layers formed primarily under the influence of high stresses become thicker in parts molded under lower injection speeds.

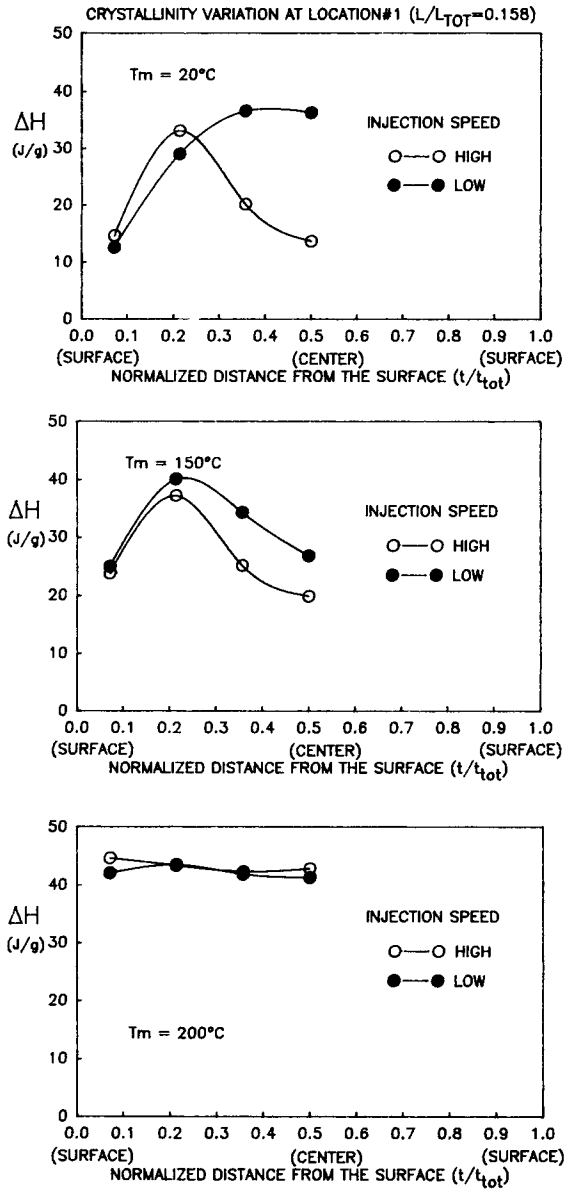

Figure 10 Crystallinity variation from skin to core (center) at location #1 showing the effect of injection speed in samples molded at (a) 20°C, (b) 150°C, and (c) 200°C mold temperatures.

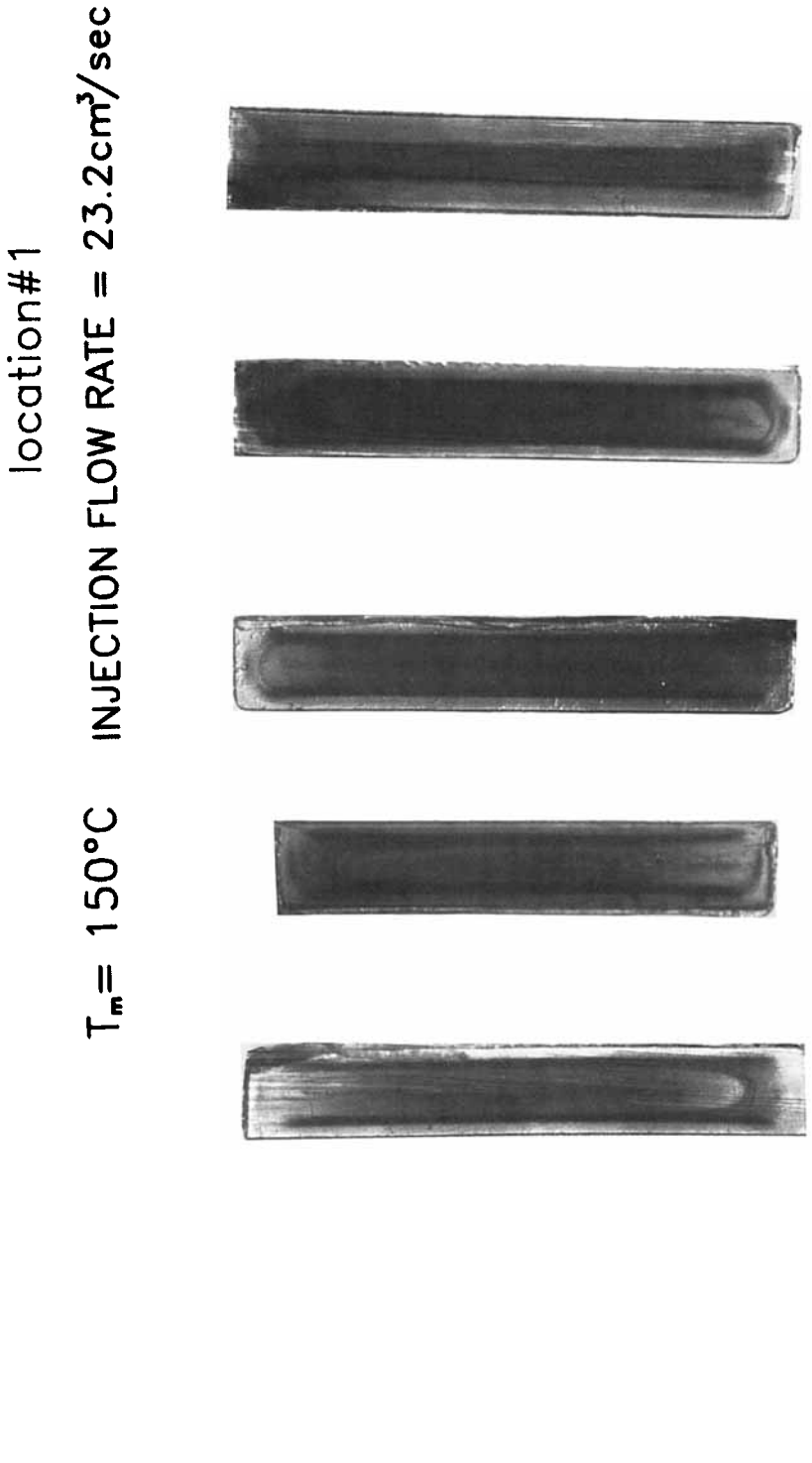

Figure 11 Optical photomicrographs of samples molded at 150°C and at different holding times and cut at location #1 with cutting procedure A (high injection speed).

Effect of Holding Time

The polymer starts to have an appreciable rate of crystallization due to thermal effects when the mold temperature is increased. This becomes substantial especially when the mold temperature is above the T_g of the polymer. The longer the part is exposed to the higher temperatures where the thermally activated crystallization is dominant, the higher the crystallinity obtained in the parts, especially in the core regions, where the material cools much slower than do the skin regions.

The T_g of PAEK is about 147°C. We chose to investigate the holding time effect at 150°C mold temperature. Figure 11 shows the cross-sectional views of these small dumbbell samples cut normal to flow direction at location #1. Holding time was varied between 30 s and 10 min. As expected, crystallinity increases with increasing holding time, especially in the core region. Figure 12 shows the results of crystallinity variations measured by DSC. As the holding time is increased, the crystallinity profiles change from a convex upward shape with a maximum at the intermediate zone to a monotonically increasing shape from skin to core, and the largest increase in crystallinities is observed in the core regions. The latter monotonically increasing crystallinity is typical of what one observes in the polymers with fast crystallization characteristics, such as PE and PP. The skin cools faster than the core, and thus it attains lower crystallinity as compared to the core regions.

WAXD Studies

Figure 13 shows the WAXS film patterns of PAEK molded at 20°C. The cutting procedure shown in Figure 2(c) was used to obtain slices at #1A–1D locations. Figures 3 and 4 show the cross-sectional view of the structures that were studied. In the samples molded at low speed, crystalline zones penetrate through to the core region. As shown in Figure 13, the WAXS pattern taken at position #1A shows the amorphous skin layer and #1B shows the oriented shear crystallized zone; interestingly, as we go further into the core region, we found that the crystalline structures in the core region are highly oriented along the flow direction (#1C, #1D). This is more evidence that the crystallization took place under stress at these regions. In the samples molded at high injection speed, the structure is composed of three layers: amorphous–crystalline–amorphous, as evidenced by the WAXS film patterns in Figure 13. The chain axes in the intermediate zone are primarily oriented along the flow direction; however, the level of orientation is small as compared to that of the core region of the low-speed molded sample. Besides, the degree of orientation seems to decrease as the distance from the surface increases (compare #1b and #1c in Fig. 13). Figure 14 shows the effect of holding time on the crystalline structure variation inside the samples molded at 150°C. It is clearly shown that as holding time is increased the perfection in crystalline structure is also increased, especially at the skin and the core regions.

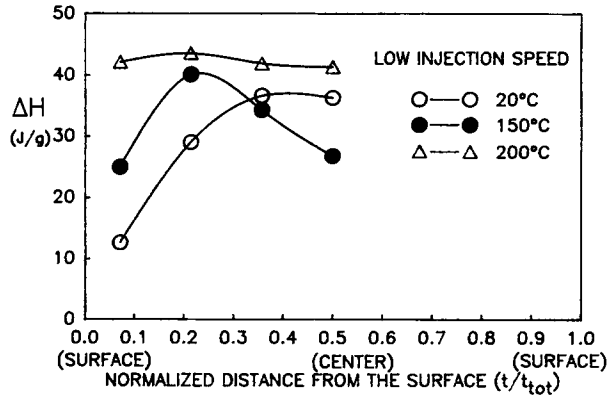

Figure 12 Crystallinity variations from skin to core in samples shown in Figure 11.

WAXS Pole Figures

To study the orientation distribution of the crystalline planes inside the injection-molded samples, WAXS pole figures were conducted for several samples cut by the procedure shown in Figure 2(c).

We chose the sample molded at 20°C (Figs. 3 and 4). Pole figures of (200) and (110) crystalline planes at the shear zone and in the core and at #1 locations are shown in Figure 15(a) and (b). In these pole figures, the spindle axes (the center of the pole figure) are along the flow direction and their left sides indicated by ND represent the normal to the wider surface of the molded bar and TD is the direction normal to the latter two axes. These pole figures indicate that the a-axes in the intermediate shear zone are oriented primarily along the normal direction and c-axes along the flow direction (with a slight tilt of the local symmetry axis toward the core). In the core region, as might be expected from the cross-sectional view and our previous WAXS film patterns, the sample molded at high speed, with an amorphous core, shows no orientation. But in the sample molded at low speed, a high orientation of

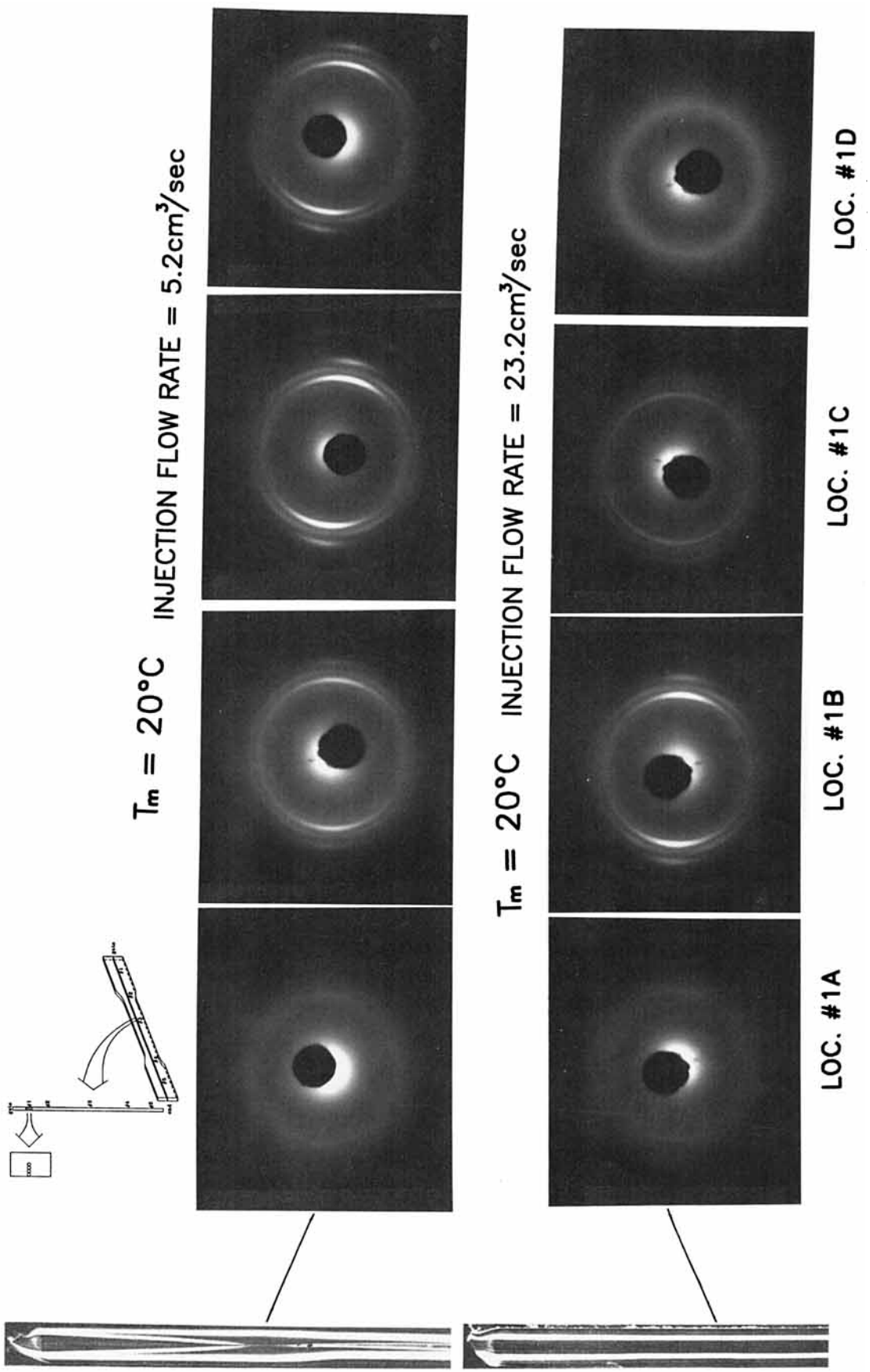

Figure 13 WAXD patterns taken at different distances from the surface at #1 location in samples molded at 20°C with low (upper row) and high (lower row) injection speeds. The exact locations where these patterns are taken are indicated on the photographic prints of the samples. Vertical direction is flow direction.

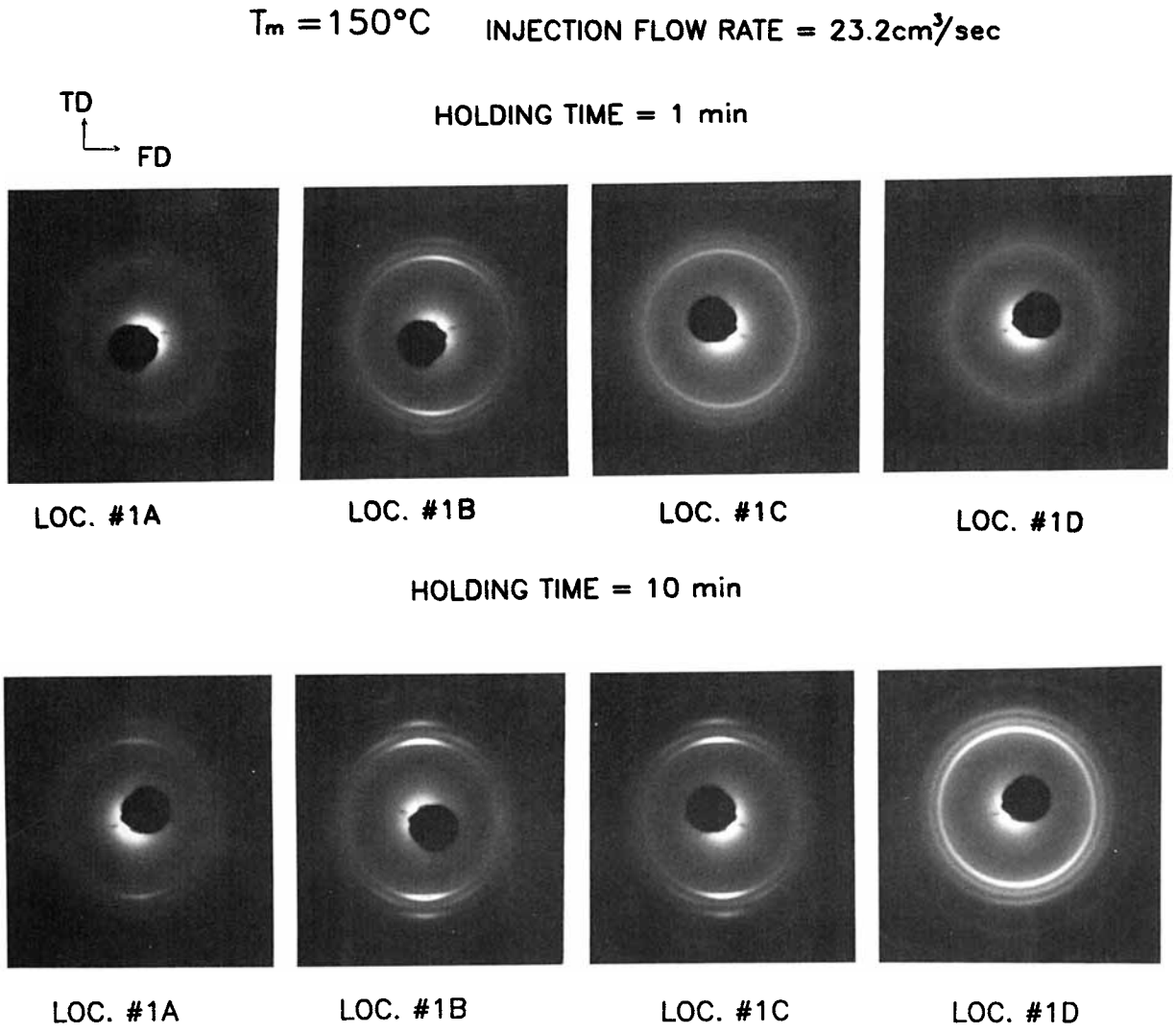

Figure 14 WAXD patterns taken at different distances from the surface at location #1 in samples molded at 150°C with 1 min (upper row) and 10 min (lower row) holding times. Injection speed is high and the flow direction is horizontal.

the c-axis pointing in the flow direction was found. In this region, the a-axes point exactly in the normal direction. This kind of finding was first reported by Lovinger and Davis[26] where flow-induced crystallization of PEEK films on a substrate was shown to yield preferred orientation of the a-axis normal to the substrate plane. Since the torsion angle [the average tilt of the phenylene rings out of the (100) plane] in the PEEK unit cell is 37°,[27] alignment of the molecule with the (100) plane parallel to the wall surface can maximize the interfacial area of contact and may, therefore, reduce the free energy for nucleation. Similar results in injection-molded PEEK have been reported in our previous paper.[12]

WAXS Film Patterns by Microcamera

Two series of WAXS film patterns by the microcamera were taken along the normal direction and at two different distances from the gate of a sample molded at 20°C and 5.2 cm^3/s. The degree of orientation of the various crystalline planes can be estimated by the azimuthal angle spread of their X-ray diffraction peaks; the narrower these peaks are, the higher the orientation. These X-ray diffraction peaks (intensity distribution along azimuthal angle) were digitized and their half-peak widths were calculated and the results were attached to the pictures in Figures 16 and 18. Figure 16 shows a picture of

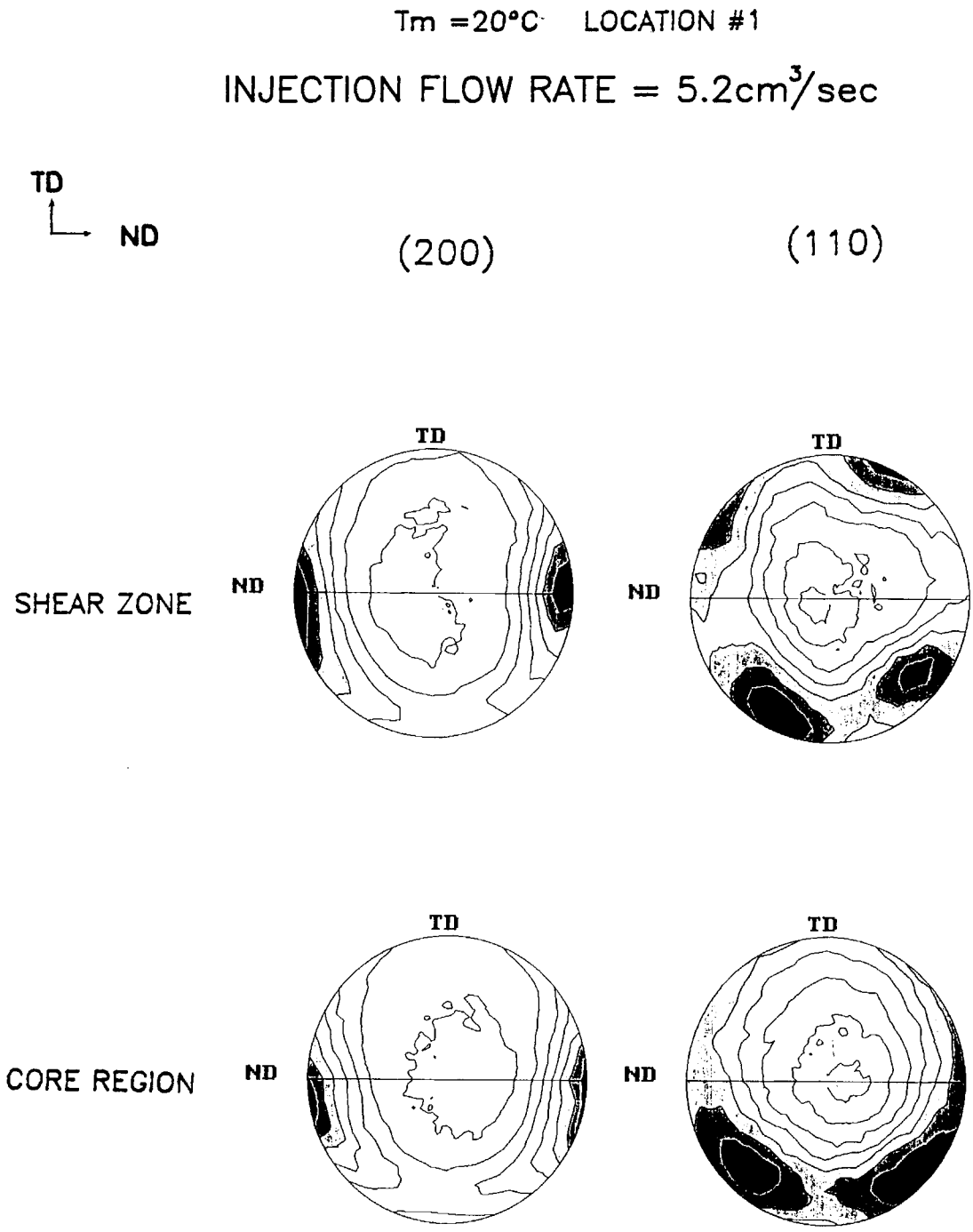

Figure 15 (a) Wide-angle X-ray pole figures of (200) and (110) planes of the samples taken at the shear crystallized intermediate zone and at the core regions (location #1 and low injection speed). (b) Wide-angle X-ray pole figures of (200) and (110) planes of the samples taken at the shear crystallized intermediate zone and at the core regions (location #1 and high injection speed).

the sample at about 11 mm from the gate. The locations that were studied by microcamera X-ray are marked by black dots. Here, the structures are very complicated. There exist five layers of structures from skin to the core. They are an amorphous skin (50 μm), a less crystallized and less oriented crys-

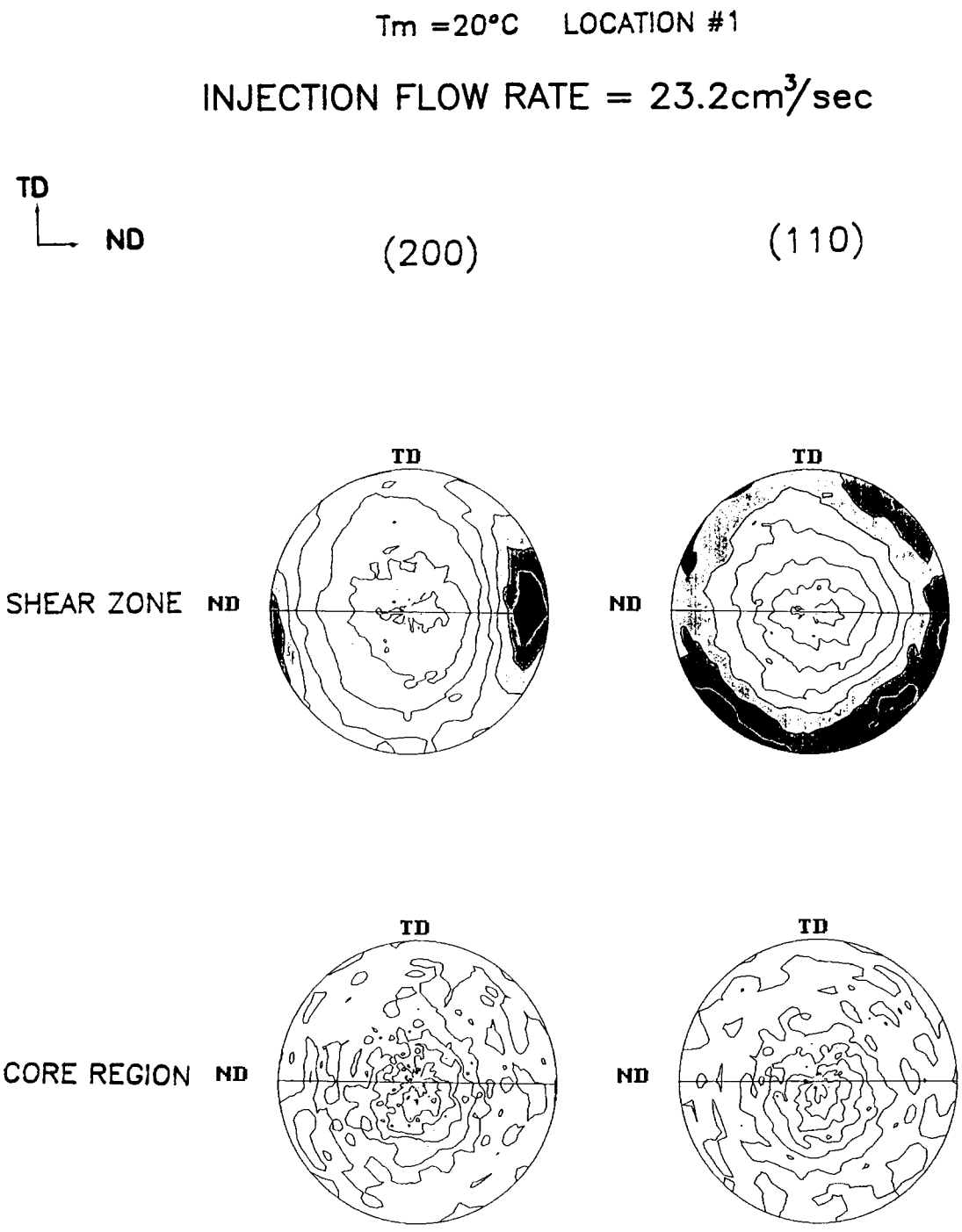

Figure 15 (*Continued from the previous page*)

talline structure (150, 250, and 350 μm), a highly crystallized and highly oriented crystalline structure (450, 550, and 650 μm), then, again, a less crystallized and less oriented crystalline structure similar to the second layer (700 and 750 μm), and, finally, an amorphous core (800 and 850 μm) (Fig. 17). Figure 18 shows the cross-sectional view of the sample cut along flow direction at a distance of about 13 mm from the gate. It shows that there exist three kinds of structure from skin to the core: an amorphous skin (50 μm), a lower crystallinity and lower-oriented crystalline structure (150 and 350 μm), and,

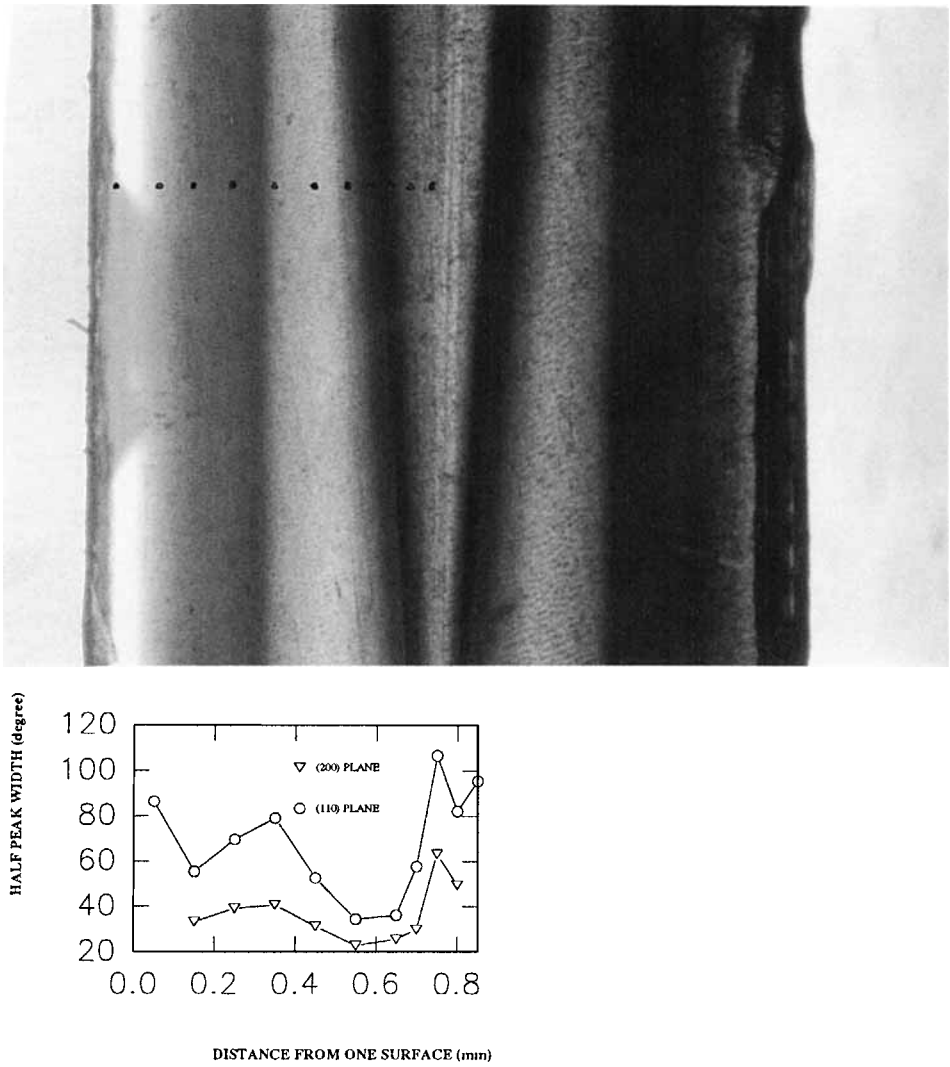

Figure 16 Optical photomicrograph and half-peak width of (200) and (110) peaks taken at different distances from the surface. The orientation data given in the lower graph are horizontally registered with the photomicrograph, indicating corresponding orientation information at given distances. Mold temperature 20°C and low injection speed; sample cut at 11 mm from the gate.

finally, a highly crystallized and highly oriented structure extended to the center of the sample (650, 750, 850, and 900 μm) (Fig. 19).

CONCLUSIONS

1. Structure gradients in injection-molded PAEK samples can be changed dramatically by the processing conditions. Samples molded at below 150°C mold temperature and high injection flow rate show a three-layer amorphous–crystalline–amorphous-type structure in the gapwise direction. Samples molded below 150°C mold temperature and at low injection speed show a more complicated multilayer structure with more crystalline layers sandwiched by amorphous layers and with these crystalline layers converging along the flow direction. When the mold temperature reaches 200°C, the structure becomes highly

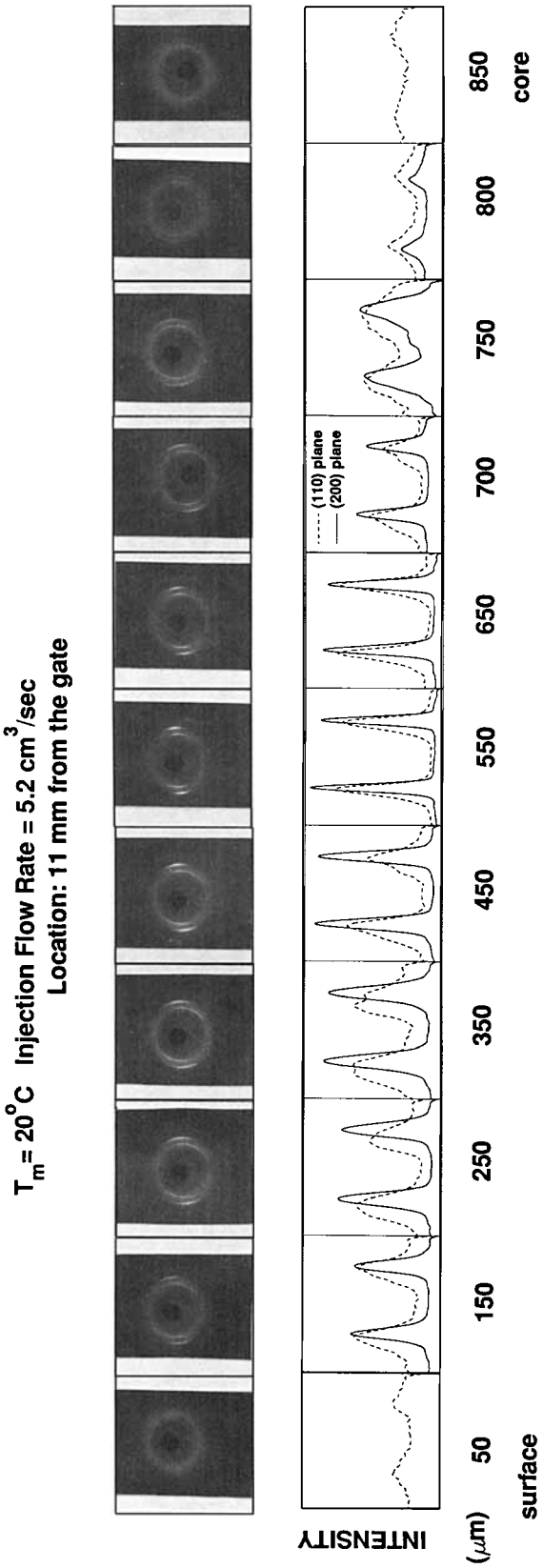

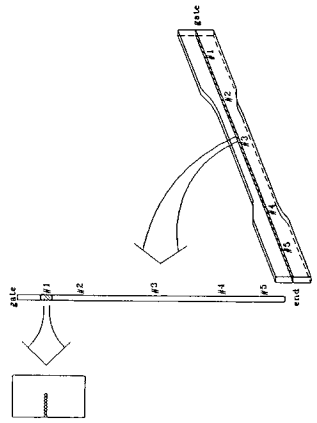

Figure 17 WAXS patterns taken with microbeam camera on sample molded at 20°C mold temperature with low injection speed (11 mm from the gate). The azimuthal distribution of intensity profiles of (110) and (200) planes are given in the lower row.

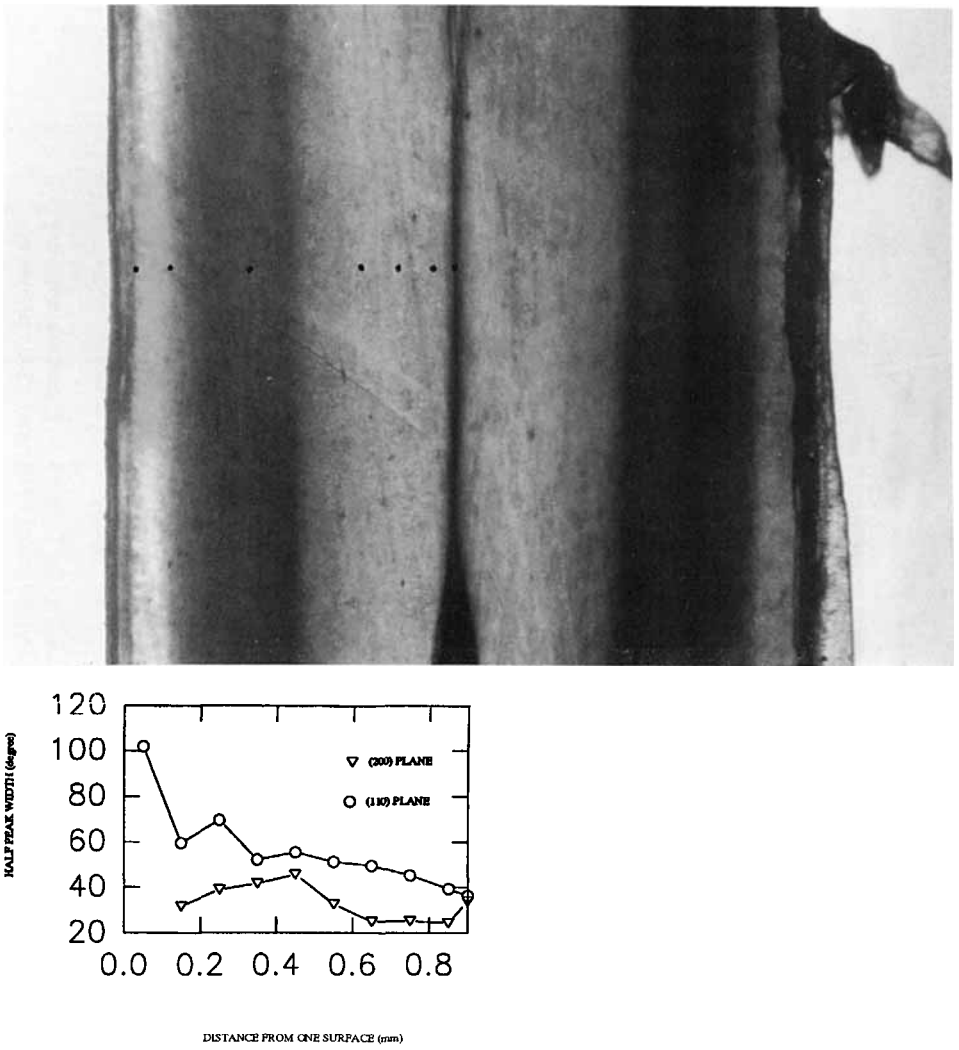

Figure 18 Optical photomicrograph and half-peak width of (200) and (110) peaks taken at different distances from the surface. The orientation data given in the lower graph are horizontally registered with the photomicrograph, indicating corresponding orientation information at given distances. Mold temperature 20°C and sample cut 13 mm from the gate where two crystallized layers merged in the core.

crystalline throughout the sample though minor variations from skin to core are observable.

2. The effects of holding time were found to be significant in samples molded at 150°C. Thermally induced crystallization increases crystallinity mostly in the core regions as the time the sample is exposed to high temperatures in the mold increased.
3. Wide-angle X-ray diffraction studies suggest that near the surface the chain axes (c-axes) are primarily oriented along the flow direction and the a-axes are perpendicular to the surface of the molded part, indicating uniplanar axial symmetry at this region. When the samples are examined at regions closer to the core region, this orientation changes from pure uniplanar–axial symmetry to isotropy at the center of the core region. A complicated multilayer structure variation along the normal direction was studied by the microcamera. Crystalline zones of different crystallinity and orientation were identified by this technique.
4. The development of the multilayer amorphous–crystalline–amorphous structure gra-

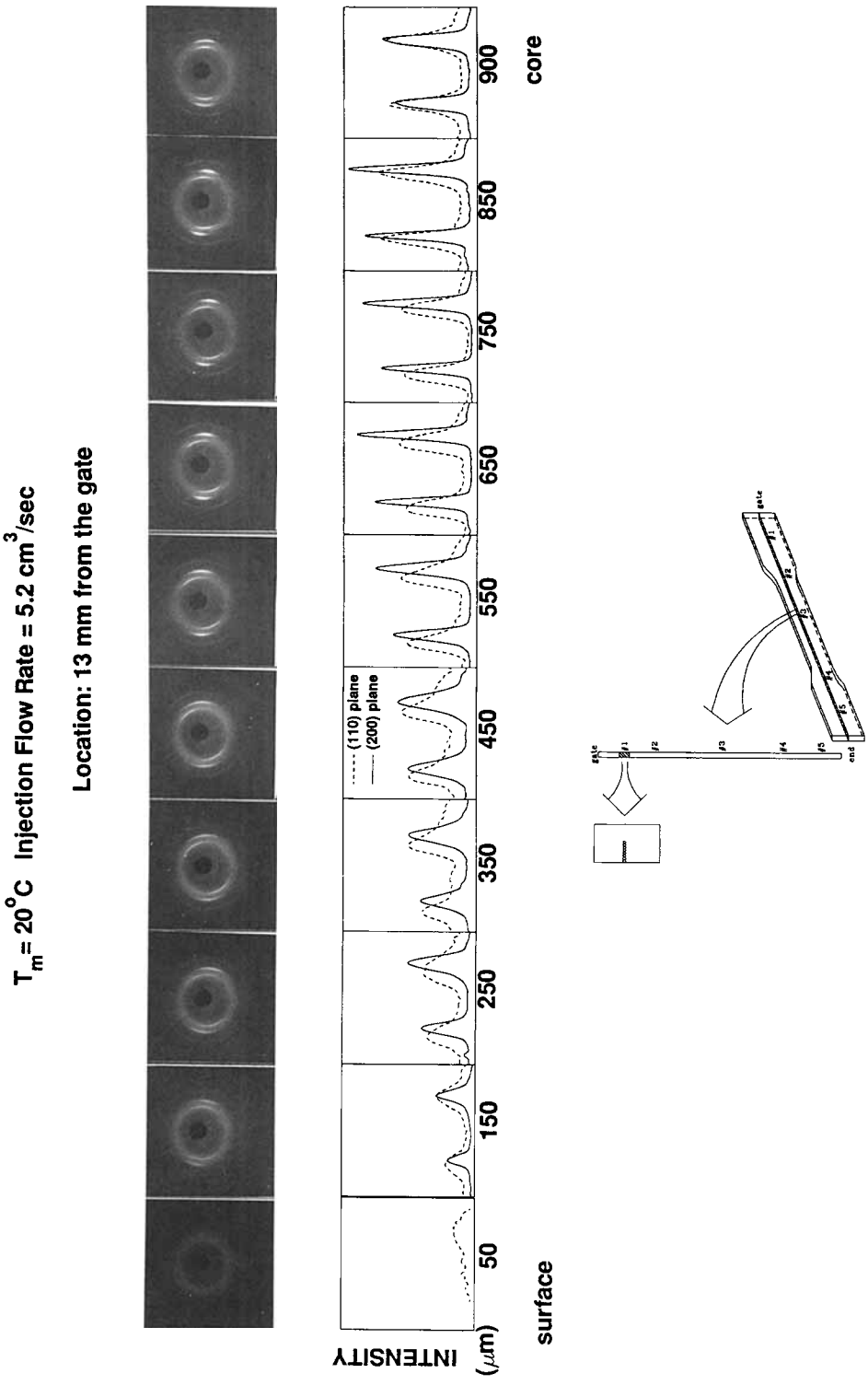

Figure 19 WAXS patterns taken with microbeam camera on sample molded at 20°C mold temperature with low injection speed (13 mm from the gate). Azimuthal distribution of intensity profiles of (110) and (200) planes are given in the lower row.

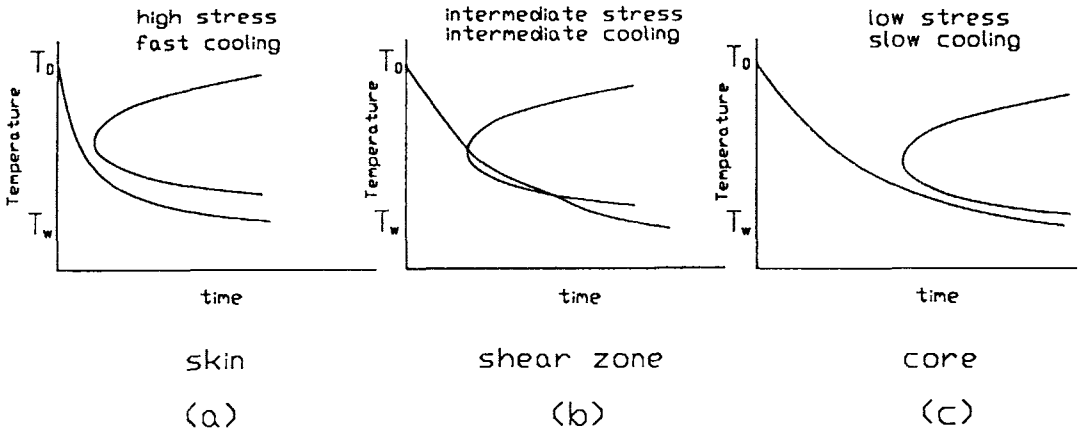

Figure 20 TTT diagrams showing the behavior at (a) skin, (b) intermediate layer, and (c) at the core in samples molded at low mold temperatures.

dient is a result of a complex interplay between the thermal and stress history. This can be explained using the TTT continuous cooling diagrams that are commonly used in metallurgy. In this diagram, the crystallization induction time envelope is drawn as a function of temperature. Figure 20 demonstrates three different conditions at low mold temperatures. Here, both the cooling curves and induction time envelopes are drawn. It is well known that under high stresses the polymers crystallize faster and at higher temperatures. Under high stresses, the induction time envelope moves to shorter times and to higher temperatures. Figure 20(a) shows the situation at the skin regions; here the cooling is very rapid. Although the induction envelope is situated at short distances, these two curves do not cross each other, and as a result, the polymer vitrifies and forms an amorphous structure. At intermediate distances from the surface [Fig. 20(b)], the polymer cools slower, due the added insulation effect of the skin, and although the induction envelope recedes to the longer times, the two curves meet together, and as a result, crystallization takes place. In the core [Fig. 20(c)] where the polymer experiences lower stresses and slower cooling rates, these curves again do not meet and the polymer cools to form an amorphous structure. The above explanation is a simplified model of what actually happens in the mold. In actuality, the induction time envelope for a given position moves dynamically in time in response to the changes in the temperature and stresses at a given location. We have built a model around this concept and successfully simulated the structural development in PEEK, which the authors published separately.[13] We currently are using the same model to simulate the structure development in PAEK.

This work was funded by the NSF Grant #DDM-8858303 Presidential Young Investigator Program.

REFERENCES

1. Y. Oyanagi and Y. Yamaguchi, *Res. Rep. Kogakuin Univ.*, **15**(14), 1 (1964).
2. B. Heise, H. G. Kilian, G. Lipke, P. Schultz, W. Woebcken, and J. Zohren, *Kolloid Z.*, **25,** 120 (1972).
3. W. Heckman and V. Johnson, *Colloid Polym. Sci.*, **252,** 826 (1974).
4. B. Heise, *Colloid Polym. Sci.*, **254,** 279 (1976).
5. R. E. Fryer, *J. Appl. Polym. Sci.*, **18,** 947 (1979).
6. M. R. Kantz, H. D. Newman, and F. H. Stigale, *J. Appl. Polym. Sci.*, **16,** 1245 (1972).
7. M. R. Kantz, *Int. J. Polym. Mater.*, **3,** 245 (1974).
8. D. R. Fitchmun and Z. Mencik, *J. Polym. Sci. Phys.*, **11,** 951 (1974).
9. K. Matsumoto, I. Miura, and K. Hayashida, *Kobunshi Ronbunshu,* **36,** 401 (1979).
10. E. S. Clark, *SPE J.*, **23,** 46 (1987).
11. C. M. Hsiung, M. Cakmak, and J. L. White, *Int. Polym. Proc.*, **5**(2), 109 (1990).
12. C. M. Hsiung, M. Cakmak, and J. L. White, *Polym. Eng. Sci.*, **30**(16), 967 (1990).

13. C. M. Hsiung and M. Cakmak, *Polym. Eng. Sci.*, **31**(19), 1372 (1991).
14. W. H. Bonner, U.S. Pat. 3,065,205 (1962).
15. R. J. Angelo, U.S. Pat. 3,767,620 (1973).
16. K. J. Dahl, U.S. Pat. 3,953,400 (1976).
17. K. J. Dahl and V. Jansons, U.S. Pat. 3,956,240 (1976).
18. K. J. Dahl, U.S. Pat. 4,247,682 (1981).
19. T. E. Attwood, P. C. Dawson, J. L. Freeman, L. R. J. Hoy, J. B. Rose, and P. A. Staniland, *Polymer*, **22**, 1096 (1981).
20. J. B. Rose and P. A. Staniland, U.S. Pat. 4,320,224 (1982).
21. L. M. Maresca, U.S. Pat. 4,339,568 (1982).
22. M. Ueda and M. Sato, *Macromolecules*, **20**, 2675 (1987).
23. H. M. Colquhoun and D. F. Lewis, *Polymer*, **29**, 1902 (1988).
24. C. M. Hsiung and M. Cakmak, *Polym. Eng. Sci.*, **31**(3), 172 (1991).
25. J. E. Harris and L. M. Robeson, *J. Polym. Sci. Part B Polym. Phys.*, **25**, 311 (1987).
26. A. J. Lovinger and D. D. Davis, *Macromolecules*, **19**(7), 1861 (1986).
27. A. V. Fratini, E. M. Cross, R. B. Whitaker, and W. W. Adams, *Polymer*, **27**, 861 (1986).

Received July 15, 1991
Accepted March 3, 1992